IEEE Access
Multidisciplinary | Rapid Review | Open Access Journal

Received 16 January 2024, accepted 25 January 2024, date of publication 30 January 2024, date of current version 8 February 2024.

Digital Object Identifier 10.1109/ACCESS.2024.3359645

METHODS

A Novel and Compact Design of High-Efficiency Broadband Rectifier for Energy Harvesting and Wireless Power Transfer

GIA THANG BUI, (Graduate Student Member, IEEE), DANG-AN NGUYEN, (Graduate Student Member, IEEE), AND CHULHUN SEO, (Senior Member, IEEE)

Department of Information and Telecommunications Engineering, Soongsil University, Seoul 06978, South Korea

Corresponding author: Chulhun Seo (chulhun@ssu.ac.kr)

This work was supported in part by the National Research Foundation of Korea (NRF) through the Korean Government (MSIP) under Grant NRF-2017R1A5A1015596.

ABSTRACT In this paper, a novel and compact structure is presented for designing a rectifier with broad operating bandwidth and high efficiency for energy harvesting and wireless power transfer based on shunt-diode configuration. Specifically, different from the conventional structure of shunt-diode configuration, the proposed structure employs a combination of two diodes and only two transmission lines that lead to a very compact size. The proposed rectifier can be matched to the source impedance when two diode branches have conjugate impedances. The admittances of two branches are analyzed based on the theory that leads to the parameters of two transmission lines can be derived by closed-forms equations. For validation, a broadband rectifier based on Schottky diode BAT15-03W was designed, simulated, fabricated, and measured showing that the rectifier can operate in the fractional bandwidth of 63.9% from 1.64 GHz to 3.18 GHZ with the condition of higher 70% power conversion efficiency or fractional bandwidth of 99.1% from 1.34 GHz to 3.97 GHz with the condition of over 50% power conversion efficiency at 13 dBm input power. Moreover, the size of the rectifier is very compact, it is recorded as only 15 mm $\times$ 14 mm. In comparison with the published broadband rectifiers, the proposed rectifier has many advantages such as smaller size and wider bandwidth.

INDEX TERMS Broadband operation, energy harvesting (EH), shunt-diode configuration, microwave rectifier, wireless power transfer (WPT).

I. INTRODUCTION

Wireless power transfer (WPT) and energy harvesting (EH) technology have been developed with great attention in recent years as it is especially useful in situations where it is unavailable or challenging to apply wire-based charging [1], [2], [3]. Besides the transmitter antenna and receiver antenna, in WPT systems, the rectifier is an indispensable ingredient for power conversion from RF to DC, and the power conversion efficiency (PCE) of the rectifier is always expected to be high value for improving WPT or EH performance [4], [5], [6]. Moreover, compact size is the general trend of current technology development, therefore, in the rectifier design, size is always a concern. In addition, depending on different applications, the operating frequency and bandwidth requirements of the rectifiers are also other, which can include types of operating frequency such as single-band [7], [8], [9], [10], [11], [12], multi-band [13], [14], [15], [16], [17], [18] and broadband [19], [20], [21], [22].

In recent years, broadband rectifier has been focused on due to they can be applied for multiple applications on researched and many reports about broadband rectifiers have been published, furthermore, for compatibility with a wide variety of applications, the compact size is important with the design of the broadband rectifier for easy integration into different systems, especially in biomedical

The associate editor coordinating the review of this manuscript and approving it for publication was Francesco G. Della Corte.

implants applications. By covering many applications such as Wifi [23], [24], [25], 3G, 4G [26], [27], [28], ISM band [29], [30], [31], and biomedical implants [32], [33], [34], the frequency range from 1.6 GHz to 3.0 GHz is chosen by many authors to realize a broadband rectifier. The impedance variation reduction mechanism was introduced in [35], [36], [37], and [38] for fundamental broadband matching but this method has bandwidth limitation due to very fast PCE drop at the two edges of the bandwidth. A high-efficiency broadband rectifier based on a low-pass filter was proposed by the author in [39], however, it is relatively large leads to not suitable for compact systems. The reported rectifier in [40] with harmonic suppression and impedance variation reduction investigation is improved in size while the bandwidth is not extended. The proposed rectifiers in [41], [42], [43], and [21] can achieve wider bandwidth and compact size based on low impedance variation of voltage doubler structure but this structure will be inefficient at low input power region due to higher saturation point.

In this report, a novel design of broadband rectifier was developed and presented with extended bandwidth while the saturation point almost does not increase for multi applications such as dedicated (short-range) WPT, indoor environment EH, and biomedical implants. The imaginary part compensation method was applied in [44], however, the rectifier in [44] was improved in wide dynamic range where the variation of the diode impedance versus input power is not large with fixed frequency and the electrical parameters of transmission lines are independent with the input power. Therefore, the wide dynamic range of the rectifier in [44] can be achieved based on imaginary part compensation with only one transmission line while achieving the imaginary part compensation in broadband is more complicated and it has not been reported. Based on the shunt-diode configuration rectifier, the proposed rectifier deploys the imaginary part compensating mechanism for impedance matching in broad bandwidth with only two transmission lines and two diodes which leads to a very compact size. A prototype of a broadband rectifier with Schottky diode BAT15-03W was fabricated and measured for proposal verification. The measurement results show that the rectifier can achieve a broad operating bandwidth of 63.9% (from 1.64 GHz to 3.18 GHz) with $>$ 70% PCE at 13 dBm input power while its dimension is only 15 mm $\times$ 14 mm. In comparison with the above-mentioned broadband rectifiers with a similar saturation point of input power, the proposed shows a wider bandwidth and a smaller size. The proposed rectifier also verified with the broadband antenna showing good working at many systems at different frequencies.

II. SHUNT-DIODE RECTIFIER OPERATION AND ANALYSIS OF PROPOSED RECTIFIER

Shunt-diode configuration is commonly employed for diode-based rectifier design in many published reports in recent years besides series-diode configuration.

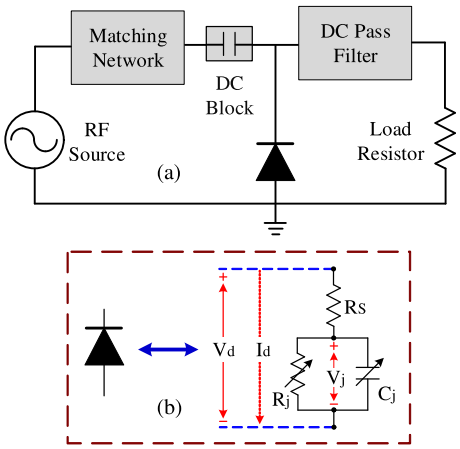

FIGURE 1. a) The conventional structure of shunt-diode configuration rectifier and b) the equivalent circuit model of the diode.

A performance comparison of these two configurations was presented in [45] showing that ideally, the shunt-diode topology and series-diode topology provide similar performance in terms of PCE. Each configuration has different advantages when in practice, the series topology PCE can be a little higher than the shunt topology due to additional losses from DC block and RF choke, however, this difference is insignificant while the shunt topology is more flexible and can be approached more easily for applying advanced structures.

A. CLASSIC SHUNT-DIODE RECTIFIER OPERATION AND POWER-DEPENDENT IMPEDANCE OF DIODE

Fig. 1a shows the conventional structure of the shunt-diode configuration rectifier where it consists of a shunt-diode, a matching network, a DC block, a DC pass filter, and the input is the RF signal from the receiver antenna, the output is DC power at the load resistor (which will be a DC-DC converter, a regulator, or a battery depending on the actual application). The diode has the equivalent circuit model as shown in Fig. 1b which comprises a series resistor (R_S), a non-linear junction capacitor (C_j), and a non-linear junction resistor (R_j). In the ideal diode operation, R_j can be assumed to be zero in forward bias and to be infinite in the opposite direction, then the idealized input RF signal voltage waveform across the diode (V) and the diode junction voltage waveform (V_d) can be described with the diode I-V curve as shown in Fig. 2 during a signal cycle. By following the analysis in [46], the calculation of the diode efficiency and diode loss can be derived as presented below. V and V_d also can be presented by equations as follows:

$$V = -V_0 + V_1 \cos(wt) \tag{1}$$

and

$$V_d = \begin{cases} -V_{d0} + V_{d1}\cos(wt - \phi)), & \text{in OFF period} \\ V_{bi}, & \text{in ON period} \end{cases} \tag{2}$$

where V_0 is the DC voltage of output power at the load resistor, V_1 is the voltage amplitude of the incident RF signal,

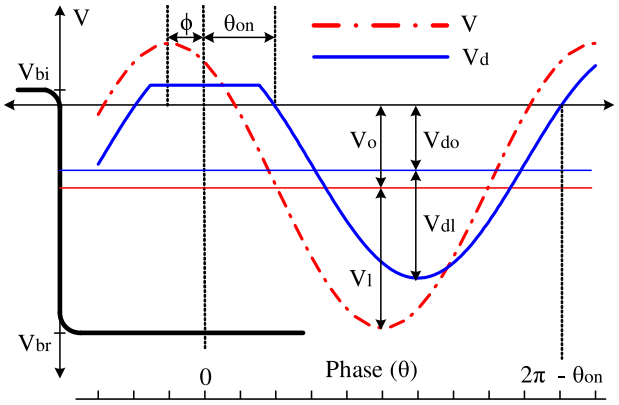

FIGURE 2. a) The idealized input RF signal voltage waveform and the diode junction voltage waveform in a rectification cycle expressed on the diode IV curve.

V_{d0} is the DC component of the diode junction voltage, V_{d1} is the voltage amplitude of fundamental frequency component of the diode junction voltage, V_{bi} and V_{br} are built-in potential voltage and breakdown voltage of the diode, respectively. As shown in Fig. 2, in comparison with incident RF signal, the phase of diode junction voltage delay angle ϕ and θ_{on} is forward-bias conduction angle of V_d. θ_{on} is a variable parameter that depends on the input power of the diode and the value of the load resistor as expressed by the below equation:

$$\tan\theta_{on} - \theta_{on} = \frac{\pi R_S}{R_L\left(1+\frac{V_{bi}}{V_0}\right)}. \tag{3}$$

where R_L is the resistance of the DC consumption output. Moreover, the power conversion efficiency (PCE) of the diode can be presented by the equation:

$$PCE(\eta) = \frac{P_{DC}}{P_{out}} = \frac{P_{DC}}{P_{DC}+P_{loss}} = \frac{1}{1+L}. \tag{4}$$

By applying the Kirchhoff's voltage law, the value of L in the equation (4) can be determined as follows:

$$L = L_1 + L_2 + L_3, \tag{5}$$

where

$$L_1 = \frac{R_L}{\pi R_S}\left(1+\frac{V_{bi}}{V_0}\right)^2\left(\theta_{on}+\frac{\theta_{on}}{2\cos^2\theta_{on}}-\frac{3}{2}\tan\theta_{on}\right), \tag{6}$$

$$L_2 = R_S R_L C_j^2 2\pi f^2\left(1+\frac{V_{bi}}{V_0}\right)\left(\frac{\pi-\theta_{on}}{\cos^2\theta_{on}}+\tan\theta_{on}\right), \tag{7}$$

and

$$L_3 = \frac{R_L}{\pi R_S}\frac{V_{bi}}{V_0}\left(1+\frac{V_{bi}}{V_0}\right)(\tan\theta_{on}-\theta_{on}), \tag{8}$$

with f is fundamental frequency and the value of the junction capacitor C_j in equation (7) is calculated as follows:

$$C_j = C_{j0}\sqrt{\frac{V_b i}{V_{bi}+|V_0|}}, \tag{9}$$

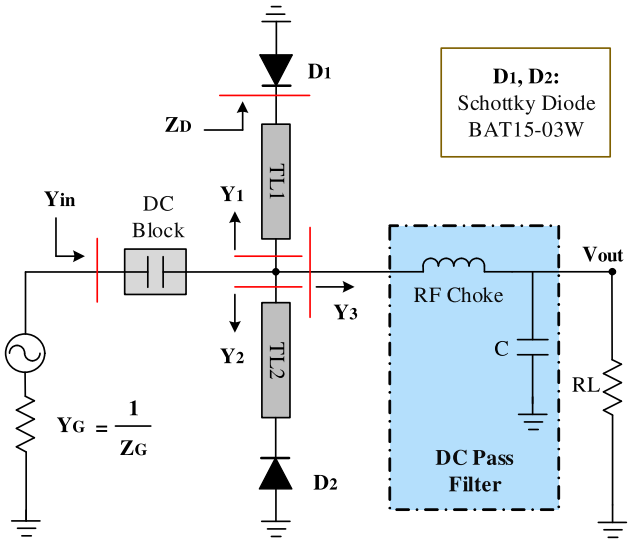

FIGURE 3. Proposed structure in detail for compact and high-efficiency broadband rectifier with only two transmission lines.

TABLE 1. Typical parameter of schottky diode BAT15-03W.

Diode Model	R_S	I_S	V_{bi}	V_{br}	C_{j0}	I_{br}
BAT15-03W	5 Ω	74 nA	0.224 V	6.4 V	138.5 fF	100 uA

where C_{j0} is the typical parameters of the diode - zero bias junction capacitance of the diode. By following the theoretical in [47], the power-dependent impedance of the diode (Z_D) at the fundamental frequency can be determined as follows:

$$Z_D = \frac{V_1}{I_r - jI_i}, \tag{10}$$

where I_r and I_i were calculated by below equations:

$$I_r = \frac{1}{\pi R_S}\int_{-\theta_{on}}^{\theta_{on}}(V-V_{bi})\cos(\theta+\phi)d\theta + \frac{1}{\pi R_S}\int_{\theta_{on}}^{2\pi-\theta_{on}}(V-V_d)\cos(\theta+\phi)d\theta, \tag{11}$$

$$I_i = \frac{1}{\pi R_S}\int_{-\theta_{on}}^{\theta_{on}}(V-V_{bi})\sin(\theta+\phi)d\theta + \frac{1}{\pi R_S}\int_{\theta_{on}}^{2\pi-\theta_{on}}(V-V_d)\sin(\theta+\phi)d\theta. \tag{12}$$

then, the power-dependent impedance of the diode will be derived by equation as follows:

$$Z_D = \frac{\pi R_S}{T\cos\theta_{on} + j2\pi f R_S C_j\left(\frac{\pi}{\cos\theta_{on}}-T\right)}. \tag{13}$$

where T is used instead of:

$$T = \frac{\theta_{on}}{\cos\theta_{on}} - \sin\theta_{on} \tag{14}$$

and θ_{on}, C_j were expressed in equations (3), (9), respectively. With f being the fundamental frequency, it can be seen that the diode impedance also depends on the operation frequency which will be a challenge to extend the operating bandwidth.

B. ANALYSIS OF PROPOSED STRUCTURE FOR BROADBAND OPERATION BASED ON IMAGINARY COMPENSATING

The structure of the proposed broad rectifier is shown in Fig. 3, different from the conventional rectifier structure, the proposed structure consists of two parallel branches of transmission line connected series with the diode. These branches have corresponding admittance Y_1 and Y_2 (two transmission line TL_1 and TL_2, two diode D_1 and D_2, respectively) as shown in Fig. 3. Then, input admittance Y_{in} will be the sum of the parallel admittances Y_1, Y_2, and Y_3:

$$Y_{in} = Y_1 + Y_2 + Y_3. \tag{15}$$

However, with very high-value inductor for RF choke, Y_3 will be approximate zero, then, Y_{in} can be considered as the sum of Y_1 and Y_2:

$$Y_{in} = Y_1 + Y_2. \tag{16}$$

Based on the theoretical of transmission line in [48], the admittance Y_1 and Y_2 of TL_1 and TL_2 series-connected with the diode can be calculated by following:

$$Y_1 = \frac{1}{Z_1}\frac{Z_1 + jZ_D\tan\theta_1}{Z_D + jZ_1\tan\theta_1}, \tag{17}$$

and

$$Y_2 = \frac{1}{Z_2}\frac{Z_2 + jZ_D\tan\theta_2}{Z_D + jZ_2\tan\theta_2}, \tag{18}$$

where Z_D is the power-dependent impedance of the diode which can be determined by equation (13), Z_1 and Z_2 are characteristic impedances, θ_1 and θ_2 are electrical lengths of corresponding transmission lines TL_1 and TL_2. Assuming that the power-dependent impedance of the diode was defined as a complex value as follows:

$$Z_D = R_D + jX_D, \tag{19}$$

with R_D is real part and X_D is imaginary, then by substituting Z_D in (19) into (17) and (18), the real parts and imaginary parts of the admittance Y_1 and Y_2 will be derived:

$$Re(Y_1) = \frac{R_D + R_D(\tan\theta_1)^2}{R_D^2 + (X_D + Z_1\tan\theta_1)^2}, \tag{20}$$

$$Re(Y_2) = \frac{R_D + R_D(\tan\theta_2)^2}{R_D^2 + (X_D + Z_2\tan\theta_2)^2}, \tag{21}$$

and

$$Im(Y_1) = \frac{(R_D^2 + X_D^2 - Z_1^2)\tan\theta_1 + Z_1X_D(\tan^2\theta_1 - 1)}{Z_1R_D^2 + Z_1(X_D + Z_1\tan\theta_1)^2}, \tag{22}$$

$$Im(Y_2) = \frac{(R_D^2 + X_D^2 - Z_2^2)\tan\theta_2 + Z_2X_D(\tan^2\theta_2 - 1)}{Z_2R_D^2 + Z_2(X_D + Z_2\tan\theta_2)^2}. \tag{23}$$

TABLE 2. Extracted parameters of two transmission line (TL_1 and TL_2) in designed rectifiers prototype.

	Z_i (Ω)	θ_i (degree) (at 1.8 GHz)	Length (initial)	Width (initial)	Length (optimized)	Width (optimized)
TL_1	125	38.57	11.36 mm	0.387 mm	11.20 mm	0.387 mm
TL_2	125	81.77	24.09 mm	0.387 mm	23.48 mm	0.387 mm

With Y_{in} was defined in (16), $Re(Y_{in})$ and $Im(Y_{in})$ can be calculated as follows:

$$Re(Y_{in}) = Re(Y_1) + Re(Y_2), \tag{24}$$

$$Im(Y_{in}) = Im(Y_1) + Im(Y_2). \tag{25}$$

Y_{in} will be matched to Y_G ($Y_G = \frac{1}{Z_G}$) when $Re(Y_{in})$ and $Im(Y_{in})$ satisfies the conditions:

$$Re(Y_{in}) = Y_G \text{ and } Im(Y_{in}) = 0. \tag{26}$$

For broadband operation rectifier, Y_{in} must be matched to Y_G in the range of fundamental frequency (f) from lowest frequency (f_1) to highest frequency (f_2). Based on equations (24), (25), and (26) where R_D and X_D will be different corresponding to the different diode impedance at each frequency, the proposed parallel structure will respond a broadband operating in the band from f_1 to f_2 when the following conditions are simultaneously satisfied:

$$Re(Y_1^{f_1}) + Re(Y_2^{f_1}) = Y_G, \tag{27}$$

$$Re(Y_1^{f_2}) + Re(Y_2^{f_2}) = Y_G, \tag{28}$$

$$Im(Y_1^{f_1}) + Im(Y_2^{f_1}) = 0, \tag{29}$$

$$Im(Y_1^{f_2}) + Im(Y_2^{f_2}) = 0, \tag{30}$$

where the value is defined at the frequency which was indicated by the superscript of the notions, real parts and imaginary parts of Y_1 and Y_2 at f_1 and f_2 were determined based on corresponding different R_D and X_D at f_1 and f_2. Then, the characteristic impedance Z_1, Z_2 and the electrical lengths θ_1, θ_2 of corresponding transmission lines TL_1, TL_2 can be determined by using *vpasolve* in MATLAB to simultaneously solve the equations (27), (28), (29), (30) with the defined values in the equations (20), (21), (22), and (23) correspond to diode impedances at two frequencies. When the input impedances were matched at f_1 and f_2, the proposed parallel structure will realize a broadband response instead of a dual-band response if the frequency $k = f_2/f_1$ is with in a certain limit. This broadband operation response can be confirmed by the simulated admittance results of designed rectifier (Shottky Diode BAT15-03W was employed) in *Advantage Keysight Systems* software from $f_1 = 1.8$ GHz to $f_2 = 3.2$ GHz as shown in Fig. 4.

As observed, the imaginary part of two admittances Y_1 and Y_2 do not vary much with the symmetrical positions on Smith Chart, that leads to the combination of these imaginary parts is almost zero. Moreover, also proven in Fig. 4, the real part of Y_1 tends to increase while the real part of Y_2 tends to decrease with increasing frequency. Therefore, with

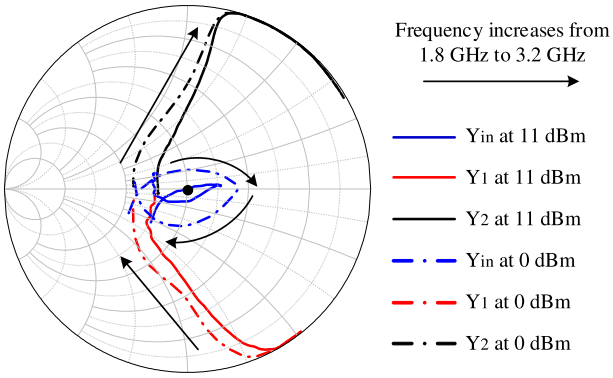

FIGURE 4. Admittance Y_{in}, Y_1, and Y_2 of simulated rectifier structure based on Schottky diode BAT15-03W.

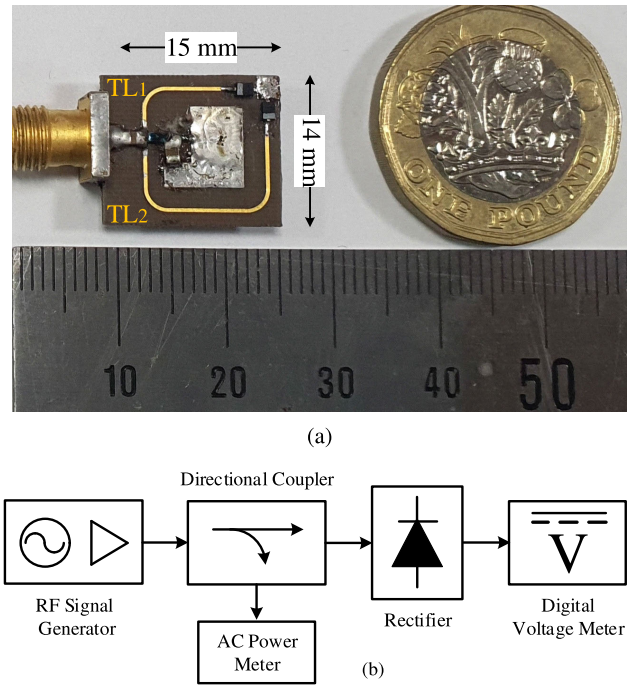

FIGURE 5. a) Photograph and dimension of fabricated rectifier and b) Block diagram of setup for rectifier measurement.

Y_{in} being matched to Y_G at two frequencies f_1 and f_2, the total real part in the frequency range from f_1 to f_2 will will varies relatively small compared to Y_G. That is reason why the impedance matching realize a broadband response instead of only dual-band response even though the parameters of transmission lines are calculated based on dual-band design. However, this broadband matching mechanism will have a certain limit on the frequency ratio k. With f_c is center frequency of operation band ($f_c = (f_1 + f_2)/2$), assuming that in the ideal case, when the imaginary parts of Y_1 and Y_2 self-compensate each other, the input impedance $Z_{in} = 1/Y_{in}$ at f_c can be calculated as follows:

$$Z_{in}^{f_c} = \frac{1}{Re(Y_1^{f_c}) + Re(Y_2^{f_c})}, \tag{31}$$

where $Re(Y_1^{f_c})$ and $Re(Y_2^{f_c})$ are also derived by equations (20) and (21). To ensure that a broadband operating can be

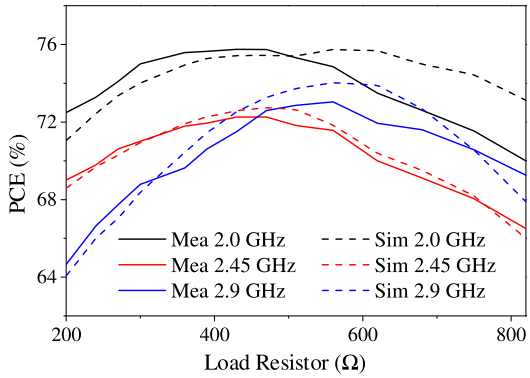

FIGURE 6. PCE versus load resistor with the input power of 11 dBm in both simulation and measurement at the different frequencies (2.0 GHz, 2.45 GHz, and 2.9 GHz).

achieved without mismatch in the range from f_1 to f_2, the frequency ratio k is limited by the value at which the input impedance Z_{in}^{fc} is obtained that satisfies the following condition:

$$\left| \frac{Z_{in}^{f_c} - Z_G}{Z_{in}^{f_c} + Z_G} \right| < \frac{1}{10} \tag{32}$$

Alternatively, the limitation of the bandwidth can also be determined by using *Advantage Keysight Systems* software to check the reflection coefficient at the center frequency f_c.

III. IMPLEMENTATION AND EXPERIMENTAL RESULTS

A. SIMULATION AND MEASUREMENT RESULTS OF DESIGNED AND FABRICATED BROADBAND RECTIFIER

Based on the presented analysis and design methodology, a broadband rectifier was designed in the operating frequency range from 1.8 GHz to 3.2 GHz (f_1 = 1.8 GHz and f_2 = 3.2 GHz). The designed broadband rectifier employs two Schottky diodes BAT15-03W whose typical parameters were presented in Table. 1. The used substrate for rectifier implementation is Taconic TLY-5 (ϵ_r = 2.2, $\tan(\delta)$ = 0.0009, 0.8 mm thickness) that can minimize PCB loss. With chosen operating frequency range and Schottky diode BAT15-03W, the parameters of two transmission lines (TL_1 and TL_2) were determined after using the optimization tool on simulation software *Advantage Keysight Systems* from calculated parameters by applying equations (27), (28), (29), and (30) and listed in Table. 2. Based on defined, the designed rectifier was simulated, fabricated, and measured.

The results of the admittances Y_1, Y_2, Y_{in} in simulation at two input power levels (0 dBm and 11 dBm) on the Admittance Smith Chart are shown in Fig. 4. It can be seen that in the range of operating frequency, the simulated admittances are matched with the presented analysis when positions of Y_1 locus and Y_2 locus are symmetric about the line with imaginary part equal zero on the Smith Chart, the sum of Y_1 and Y_2 is Y_{in} will be located around the center of the Smith Chart, which means that the proposed rectifier will be matched to the source impedance of 50 Ω in the operating frequency range. With imaginary

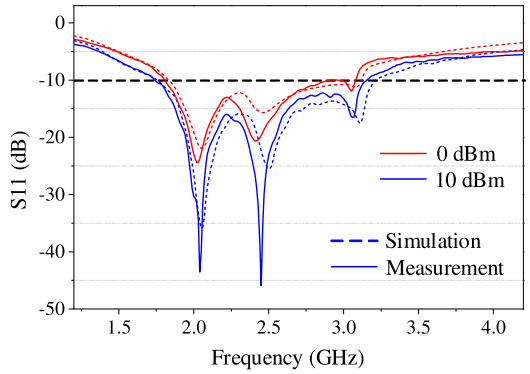

FIGURE 7. Reflection coefficient of proposed rectifier at $R_L = 510\Omega$ and two input power level (0 dBm and 10 dBm) for both simulation and measurement.

part compensating mechanism and presented admittances in Fig. 4, it can be seen that power delivered to each diode is similar. Moreover, the variation of diode impedance versus delivered power is not much when the different between admittances is small with two input power level of 0 dBm and 11 dBm. It indicates that with small delivered power differences, about few dBm, the change of the diode impedance is insignificant. Fig. 5a shows the photograph of the fabricated rectifier prototype which was used to measure for verification. As observed, the fabricated rectifier has a very small dimension of only 15 mm × 14 mm, which means the proposed broadband rectifier can be easily integrated into many different systems or devices depending on different applications and frequencies. Different from the simulation with the idea of RF choke and DC block, in reality, the DC pass filter of fabricated rectifier is formed by a combination of a 100 nH series-inductor (LQW18ANR10G00) by muRata and a 2400 pF parallel-capacitor (C08BL242X-5UN-X0T) by Knowles Lab. The broadband rectifier was measured by measurement setup as shown in Fig. 5b where the source generator Agilent N5182A generates the RF signal to the directional coupler, then RF signal is transmitted to the rectifier and the amplitude of RF signal measured at the rectifier. Finally, the output DC voltage is measured at a digital voltage meter to calculate PCE by following below equations:

$$PCE(\eta) = \frac{P_{DC}}{P_{in}} \times 100\% = \frac{V_{DC}^2}{R_L P_{in}} \times 100\%. \qquad (33)$$

where P_{DC} is the output power (Watt), P_{in} is the input power (Watt), V_{DC} is the DC voltage (V) measured at the digital voltage meter and R_L is the resistance value of load (Ω).

The optimal value of the load resistor can be determined by resistor sweeping in both simulation and measurement, Fig. 6 depicts the PCE versus load resistor with the input power of 11 dBm in both simulation and measurement at three different frequencies 2.0 GHz, 2.45 GHz, and 2.9 GHz. It can be seen that PCE will be optimized with the load resistor in the range from around 400 Ω to 600 Ω. Accordingly, in this report, the load resistor 510 Ω was used to determine PCE for

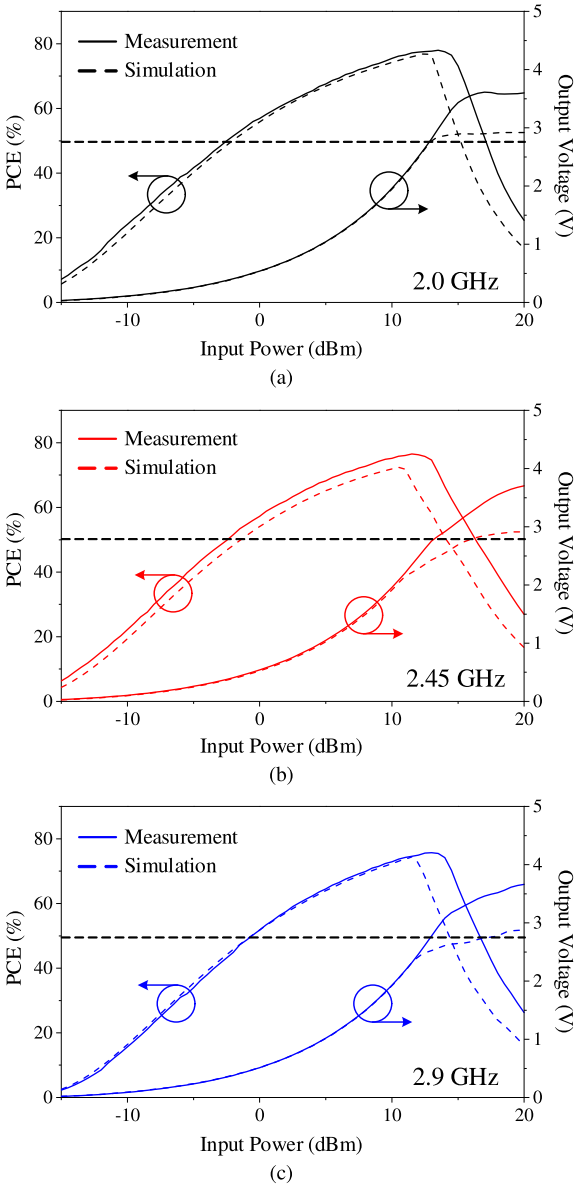

FIGURE 8. a) PCE and output voltage versus input power levels at a) 2.0 GHz, b) 2.45 GHz, and c) 2.9 GHz with $R_L = 510\Omega$ for both simulation and measurement.

both simulation and measurement. The reflection coefficient (S_{11}) in measurement is measured by the network analyzer Protek A338 and plotted in Fig. 7 along with the S_{11} in simulation at two different input power levels (0 dBm and 10 dBm). As observed, at 10 dBm input power, the measured S_{11} is lower than < -10 dB from 1.74 GHz to 3.16 GHz while the simulated S_{11} has the value below < -10 dB from 1.76 GHz to 3.21 GHz the indicates a good matching between simulation and measurement and a good broadband operating of the proposed rectifier although the measured S_{11} has some better resonance points but the bandwidth is a bit narrower in comparison with the simulated S_{11}. This slight difference can be explained by the fact that the diode model used in the simulation based on the parameters given by the manufacturer is only relative to the actual diode model, which cannot be

TABLE 3. Comparison of the proposed broadband rectifier in this paper with the published rectifiers at similar input power level.

Ref.	Year	PCE Condition	Frequency Range (GHz)	Fractional Bandwidth	Input Power	Peak PCE (dBm)	Schottky Diode	Dimension (mm^2)	Wavelength Size (λ^2)
[35]	2017	$> 70\%$	$2.08 - 2.58$	21.5%	15.5 dBm	80.8%	HSMS 286F	8568	0.6337
[36]	2018	$> 70\%$	$0.57 - 0.9$	44.9%	12.8 dBm	76%	HSMS 2860	6016	0.0541
[37]	2019	$> 70\%$	$2.0 - 3.05$	41.5%	10 dBm	75.8%	HSMS2860	1260	0.1302
[38]	2020	$> 70\%$	$2.1 - 3.3$	44.4%	14 dBm	76.3%	HSMS2850	558	0.0675
[39]	2022	$> 70\%$	$1.7 - 2.8$	48.9%	12 dBm	82.5%	HSMS2860	1472	0.1282
[40]	2023	$> 70\%$	$1.77 - 2.85$	46.8%	11.5 dBm	82.3%	BAT15-03W	513	0.0463
This work	2023	$> 70\%$	$1.64 - 3.18$	63.9%	13 dBm	81.8%	BAT15-03W	210	0.0236

λ: Wavelength at the highest frequency of operating frequency range

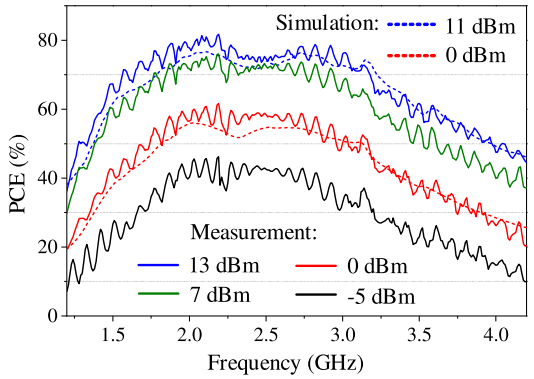

FIGURE 9. PCE versus frequencies in simulation at 0 dBm, 11 dBm and PCE versus frequencies in measurement at 13 dBm, 7 dBm, 0 dBm, and -5 dBm.

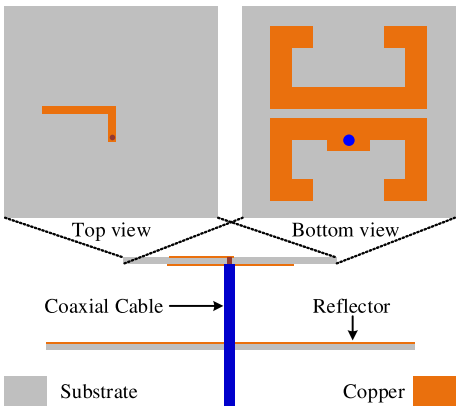

FIGURE 10. Detail structure of broadband antenna employed for rectifier verification.

guaranteed absolutely accuracy. At 0 dBm input power, both simulated and measured S_{11} are a little higher than the one at 10 dBm, however, the bandwidth is quite similar with the S_{11} at 10 dBm input power. Fig. 8 presents the PCE and output voltage versus input power levels at three frequencies: a) 2.0 GHz, b) 2.45 GHz, and 2.9 GHz. It can be seen that at 2.0 GHz and 2.9 GHz, the PCE in simulation is similar to the PCE in the measurement while the PCE in measurement is slightly higher than the PCE in simulation at 2.45 GHz due to better resonance S_{11} at 2.45 GHz in measurement. Furthermore, at all three frequencies, the measured results have a saturation point higher than the simulated results due to the accuracy diode model usually has breakdown voltage (V_{br}) higher than the one of the diode model in simulation when the simulated PCE peak at around 11 dBm (about 70% - 75%) while the PCE in measurement is highest at around 13 dBm (about 75% - 80%).

The PCE versus frequencies of the proposed rectifier at different input power levels in both simulation and measurement are depicted in Fig. 9 where the PCEs in measurement have some ripples. There are many issues that can lead to these ripples such as diode model, fabrication tolerance, environmental, quality of solder joints, signal instability from generator, coaxial cables…etc which can not be controlled. However, the amplitude of these ripples is not too large so it is acceptable. In addition, despite the ripples, PCEs versus frequencies still have the forms quite similar to simulation results. With 11 dBm in simulation and 13 dBm in measurement for highest PCE as shown in Fig. 9, the over 70% PCE can be achieved from 1.79 GHz to 3.22 GHz (corresponding to fractional bandwidth of 57.1%) in simulation at 11 dBm input power while in measurement, this range is from 1.64 GHz to 3.18 GHz (corresponding to fractional bandwidth of 63.9%) at 13 dBm input power with the peak PCE is 81.8% at 2.19 GHz. Moreover, at these input power levels, the PCE can be higher than 50% from 1.38 GHz to 3.96 GHz (96.6% fractional bandwidth) in simulation and from 1.34 GHz to 3.97 GHz (99.1% fractional bandwidth) in measurement. In addition, as exhibited in Fig. 9, at low input power levels, the proposed rectifier can still provide good performance in broadband such as about 50% at 0 dBm or 30% at -5 dBm. It can be seen that the proposed rectifier is suitable for application to wireless power transmission or energy harvesting in the indoor environment. To clarify the advantages of the proposed broadband rectifier, a comparison between the rectifier in this paper and published broadband rectifiers that have similar input power levels is summarized

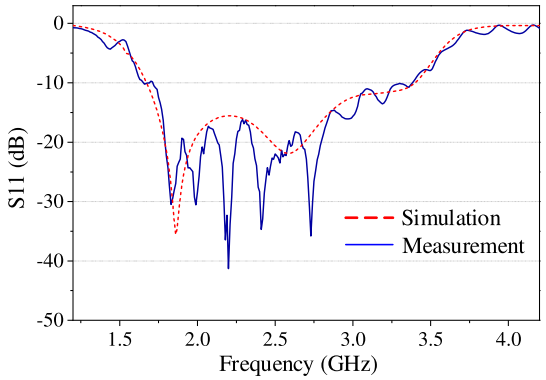

FIGURE 11. Reflection coefficient S_{11} of broadband antenna employed for rectifier verification.

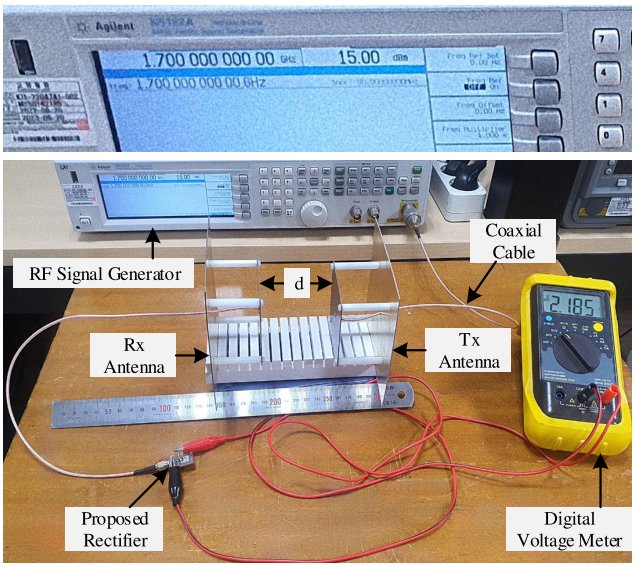

FIGURE 12. System setup for wireless power transfer efficiency measurement include transmitter antenna, receiver antenna, and rectifier.

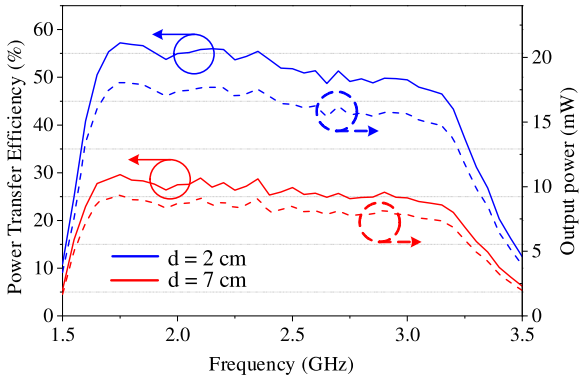

FIGURE 13. Measured power transfer efficiency and output power of WPT system versus frequency at two distances 7 cm and 2 cm.

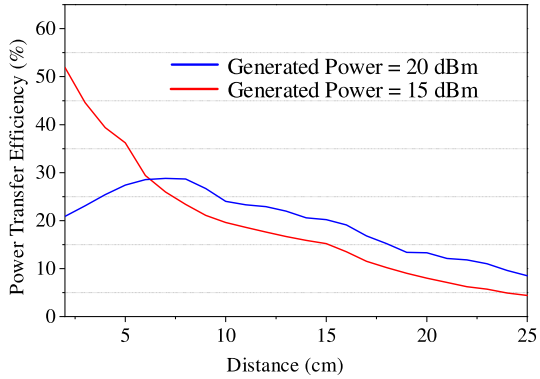

FIGURE 14. Measured power transfer efficiency and of WPT system versus distances of antennas at frequency 2.45 GHz with two generated power levels of 20 dBm and 15 dBm.

and presented in Table. 3. As noticed, with similar input power and peak PCE, the proposed rectifier has a very wide fractional bandwidth (wider than bandwidth of all papers listed in Table. 3 which can completely meet broadband criteria) while its dimension and size according to wavelength are superiorly smaller. By applying imaginary compensation mechanism, the rectifier can achieve good results while the structure is very minimal, which is best shown through the comparison in Table. 3 with the reports on broadband rectifiers published in recent years.

B. IMPLEMENTATION OF PROPOSED RECTIFIER IN WPT SYSTEM

For further verification, a broadband antenna was fabricated for WPT system implementation with the proposed rectifier. The broadband antenna was designed by following [49] which has the detailed structure shown in Fig. 10 and the substrate used for antenna fabrication is Taconic TLC-32 ($\epsilon_r = 3.2$, $\tan(\delta) = 0.003$, 0.8 mm thickness). Fig. 11 plots the simulated and measured reflection coefficient S_{11} of the designed broadband antenna. As shown in Fig. 11, the fabricated antenna can operate in broadband from 1.72 GHz to 3.38 GHz with $S_{11} < -10$ dB. Fig. 12 shows the system setup of power transfer efficiency (PTE) measuring where the fabricated broadband antenna was applied for both the transmitter antenna and receiver antenna. The power transfer efficiency of the system and output power were calculated through output DC voltage measured by a digital voltage meter at the load resistor of the proposed rectifier by the below equation:

$$P_{out} = \frac{V_{DC}^2}{R_L} \text{ and } \eta_{PT} = \frac{P_{out}}{P_{GP}} \times 100\%. \quad (34)$$

where P_{out} is output power and η_{PT} is power transfer efficiency, V_{DC} is measured DC voltage at the load resistor (R_L), and P_{GP} is generated power, then, the power transfer efficiency is calculated based on the total system loss including insertion loss of two cables, the free space loss between the two antennas, and the rectifier loss. These measured results of the system versus frequencies are depicted in Fig. 13 with the generated power of 15 dBm from the signal generator. As observed, when the distance between the transmitter antenna and the receiver antenna is 2 cm, the power transfer efficiency is approximately 55% in the frequency range from 1.7 GHz to 3.2 GHz

while this frequency range also exhibits around 30% power transfer efficiency with 7 cm distance. Fig. 14 shows the efficiencies of the system at frequency 2.45 GHz with two generated power levels of 20 dBm and 15 dBm that indicates the proposed rectifier is good WPT-capable. With meter scale or more of two antennas, this system with the proposed rectifier can still ensure good operation but the power level at the transmitting antenna needs to be higher, which leads to the need to add an additional power amplifier between the generator and the transmitting antenna due to the output power limitation of generator. It indicates that the proposed rectifier is suitable for many applications at different frequencies.

IV. CONCLUSION

This article proposes a novel structure for designing broadband rectifiers with high PCE and compact size based on shunt-diode configuration and a prototype has been a successful realization to measure for verification. Different from conventional shunt-diode topology, the proposed broadband rectifier uses two parallel diode branches with two series transmission lines to compensate for the imaginary part. The analysis of the power-dependent impedance of the diode has been extracted, then the parameters of two transmission lines can be derived by closed-form equations based on diode power-dependent impedance. In the implementation, the fabricated rectifier indicates superior measurement results when compared to the published broadband rectifiers in a similar effective input power range. The measured results show that the proposed has a high PCE in a wider fractional bandwidth with the smallest size in both physical dimensions and according to the wavelength. Moreover, at two edges of the bandwidth, the PCE drops slowly which indicates the proposed broadband rectifier can achieve an acceptable PCE in ultra-wideband. In addition, the implemented rectifier has been verified in a broadband WPT system where a broadband antenna was fabricated and used for both the transmitter antenna and receiver antenna. The high measured PTE of the system in a wide range of frequencies demonstrates that the proposed broadband rectifier can be easily applied for many applications at different frequencies.

REFERENCES

[1] W. C. Brown, "The history of power transmission by radio waves," *IEEE Trans. Microw. Theory Techn.*, vol. MTT-32, no. 9, pp. 1230–1242, Sep. 1984.

[2] K. M. Z. Shams and M. Ali, "Wireless power transmission to a buried sensor in concrete," *IEEE Sensors J.*, vol. 7, no. 12, pp. 1573–1577, Dec. 2007, doi: 10.1109/JSEN.2007.908230.

[3] X. Wang and A. Mortazawi, "Rectifier array with adaptive power distribution for wide dynamic range RF-DC conversion," *IEEE Trans. Microw. Theory Techn.*, vol. 67, no. 1, pp. 392–401, Jan. 2019.

[4] D. M. Nguyen, N. D. Au, and C. Seo, "A microwave power transmission system using sequential phase ring antenna and inverted class F rectenna," *IEEE Access*, vol. 9, pp. 134163–134173, 2021.

[5] J. Guo, H. Zhang, and X. Zhu, "Theoretical analysis of RF-DC conversion efficiency for class-F rectifiers," *IEEE Trans. Microw. Theory Techn.*, vol. 62, no. 4, pp. 977–985, Apr. 2014.

[6] S. Abbasian and T. Johnson, "Power-efficiency characteristics of class-F and inverse class-F synchronous rectifiers," *IEEE Trans. Microw. Theory Techn.*, vol. 64, no. 12, pp. 4740–4751, Dec. 2016.

[7] D.-A. Nguyen, G. T. Bui, H. Nam, Y. Kim, and C. Seo, "A 433-MHz compact inverse class-F rectifier for biomedical wireless power transmission," *IEEE Microw. Wireless Technol. Lett.*, vol. 33, no. 6, pp. 759–762, Jun. 2023.

[8] Z. He, H. Lin, and C. Liu, "A novel class-C rectifier with high efficiency for wireless power transmission," *IEEE Microw. Wireless Compon. Lett.*, vol. 30, no. 12, pp. 1197–1200, Dec. 2020.

[9] F. Zhao, D. Inserra, G. Wen, J. Li, and Y. Huang, "A high-efficiency inverse class-F microwave rectifier for wireless power transmission," *IEEE Microw. Wireless Compon. Lett.*, vol. 29, no. 11, pp. 725–728, Nov. 2019.

[10] N. Sakai, K. Noguchi, and K. Itoh, "A 5.8-GHz band highly efficient 1-W rectenna with short-stub-connected high-impedance dipole antenna," *IEEE Trans. Microw. Theory Techn.*, vol. 69, no. 7, pp. 3558–3566, Jul. 2021.

[11] C. Liu, F. Tan, H. Zhang, and Q. He, "A novel single-diode microwave rectifier with a series band-stop structure," *IEEE Trans. Microw. Theory Techn.*, vol. 65, no. 2, pp. 600–606, Feb. 2017.

[12] M.-D. Wei, Y.-T. Chang, D. Wang, C.-H. Tseng, and R. Negra, "Balanced RF rectifier for energy recovery with minimized input impedance variation," *IEEE Trans. Microw. Theory Techn.*, vol. 65, no. 5, pp. 1598–1604, May 2017.

[13] D.-A. Nguyen, G. T. Bui, H. Nam, and C. Seo, "Design of dual-band inverse class-F rectifier for wireless power transfer and energy harvesting," *IEEE Microw. Wireless Technol. Lett.*, vol. 33, no. 3, pp. 355–358, Mar. 2023.

[14] G. T. Bui, D.-A. Nguyen, and C. Seo, "A novel design of dual-band inverse class-F shunt-diode rectifier for energy harvesting," *IEEE Trans. Circuits Syst. II, Exp. Briefs*, early access, Jan. 30, 2023, doi: 10.1109/TCSII.2023.3240501.

[15] M. A. Halimi, D. Surender, T. Khan, A. A. Kishk, and S. R. Rengarajan, "A multistepped transmission line matching strategy based triple-band rectifier for RFEH/WPT applications," *IEEE Microw. Wireless Compon. Lett.*, vol. 32, no. 8, pp. 1007–1010, Aug. 2022.

[16] G. T. Bui, D.-A. Nguyen, and C. Seo, "A highly efficient design of 2.45/5.8-GHz dual-band class-F shunt-diode rectifier for wireless power transmission," *IEEE Microw. Wireless Technol. Lett.*, vol. 33, no. 4, pp. 495–498, Apr. 2023.

[17] K. Bhatt, S. Kumar, P. Kumar, and C. C. Tripathi, "Highly efficient 2.4 and 5.8 GHz dual-band rectenna for energy harvesting applications," *IEEE Antennas Wireless Propag. Lett.*, vol. 18, pp. 2637–2641, 2019.

[18] H. Sun, Y. Guo, M. He, and Z. Zhong, "A dual-band rectenna using broadband Yagi antenna array for ambient RF power harvesting," *IEEE Antennas Wireless Propag. Lett.*, vol. 12, pp. 918–921, 2013.

[19] M. M. Mansour and H. Kanaya, "Compact and broadband RF rectifier with 1.5 octave bandwidth based on a simple pair of L-section matching network," *IEEE Microw. Wireless Compon. Lett.*, vol. 28, no. 4, pp. 335–337, Apr. 2018.

[20] C. Song, Y. Huang, J. Zhou, J. Zhang, S. Yuan, and P. Carter, "A high-efficiency broadband rectenna for ambient wireless energy harvesting," *IEEE Trans. Antennas Propag.*, vol. 63, no. 8, pp. 3486–3495, Aug. 2015.

[21] W. Liu, K. Huang, T. Wang, J. Hou, and Z. Zhang, "Broadband high-efficiency RF rectifier with a cross-shaped match stub of two one-eighth-wavelength transmission lines," *IEEE Microw. Wireless Compon. Lett.*, vol. 31, no. 10, pp. 1170–1173, Oct. 2021.

[22] J. Liu, M. H. Zhang, S. T. Cai, and J. F. Chen, "A broadband rectifier with wide incident angle of incoming waves based on quadrature coupler for RF energy harvesting," *IEEE Microw. Wireless Compon. Lett.*, vol. 32, no. 12, pp. 1483–1486, Dec. 2022.

[23] Y. Cui, X. Wang, G. Shen, and R. Li, "A triband SIW cavity-backed differentially fed dual-polarized slot antenna for WiFi/5G applications," *IEEE Trans. Antennas Propag.*, vol. 68, no. 12, pp. 8209–8214, Dec. 2020.

[24] J. Qi, Q. Wang, F. Deng, Z. Zeng, and J. Qiu, "Low-profile uni-cavity high-gain FPC antenna covering entire global 2.4 GHz and 5 GHz WiFi-bands using uncorrelated dual-band PRS and phase compensation AMC," *IEEE Trans. Antennas Propag.*, vol. 70, no. 11, pp. 10187–10198, Nov. 2022.

[25] M. E. de Cos, M. Mantash, A. Tarot, and F. Las-Heras, "Dual-band coplanar waveguide-fed smiling monopole antenna for WiFi and 4G long-term evolution applications," *IET Microw., Antennas Propag.*, vol. 7, no. 9, pp. 777–782, Jun. 2013.

[26] S. X. Ta, D. M. Nguyen, K. K. Nguyen, C. Dao-Ngoc, and N. Nguyen-Trong, "A tripolarized antenna with ultrawide operational bandwidth," *IEEE Trans. Antennas Propag.*, vol. 68, no. 6, pp. 4386–4396, Jun. 2020.

[27] H. Liu, C. Zhai, and K. M. Cheng, "Novel dual-band equal-cell Doherty amplifier design with extended power back-off range," *IEEE Trans. Microw. Theory Techn.*, vol. 68, no. 3, pp. 1012–1021, Mar. 2020.

[28] L. Wu, R. Li, Y. Qin, and Y. Cui, "Bandwidth-enhanced broadband dual-polarized antennas for 2G/3G/4G and IMT services," *IEEE Antennas Wireless Propag. Lett.*, vol. 17, no. 9, pp. 1702–1706, Sep. 2018.

[29] T. Ngo and Y.-X. Guo, "Harmonic-recycling rectifier for high-efficiency far-field wireless power transfer," *IEEE Trans. Circuits Syst. II, Exp. Briefs*, vol. 67, no. 4, pp. 770–774, Apr. 2020.

[30] Z.-X. Du and X. Y. Zhang, "High-efficiency single- and dual-band rectifiers using a complex impedance compression network for wireless power transfer," *IEEE Trans. Ind. Electron.*, vol. 65, no. 6, pp. 5012–5022, Jun. 2018.

[31] D. Wang and R. Negra, "Design of a rectifier for 2.45 GHz wireless power transmission," in *Proc. 8th Conf. Ph.D. Res. Microelectron. Electron.*, Aachen, Germany, Jun. 2012, pp. 1–4.

[32] H. Le-Huu and C. Seo, "Bipolar concentric-loop midfield transmitter for high-performance wireless power transfer to biomedical implants," in *Proc. Wireless Power Week (WPW)*, Bordeaux, France, Jul. 2022, pp. 275–279.

[33] A. Iqbal, M. Al-Hasan, I. B. Mabrouk, A. Basir, M. Nedil, and H. Yoo, "Biotelemetry and wireless powering of biomedical implants using a rectifier integrated self-diplexing implantable antenna," *IEEE Trans. Microw. Theory Techn.*, vol. 69, no. 7, pp. 3438–3451, Jul. 2021.

[34] H. Le-Huu and C. Seo, "Bipolar spiral midfield wireless power transfer for cardiac implants application," *IEEE Antennas Wireless Propag. Lett.*, vol. 20, no. 9, pp. 1631–1635, Sep. 2021.

[35] X. Y. Zhang, Z.-X. Du, and Q. Xue, "High-efficiency broadband rectifier with wide ranges of input power and output load based on branch-line coupler," *IEEE Trans. Circuits Syst. I, Reg. Papers*, vol. 64, no. 3, pp. 731–739, Mar. 2017.

[36] Y. L. Lin, X. Y. Zhang, Z.-X. Du, and Q. W. Lin, "High-efficiency microwave rectifier with extended operating bandwidth," *IEEE Trans. Circuits Syst. II, Exp. Briefs*, vol. 65, no. 7, pp. 819–823, Jul. 2018.

[37] P. Wu, S. Y. Huang, W. Zhou, W. Yu, Z. Liu, X. Chen, and C. Liu, "Compact high-efficiency broadband rectifier with multi-stage-transmission-line matching," *IEEE Trans. Circuits Syst. II, Exp. Briefs*, vol. 66, no. 8, pp. 1316–1320, Aug. 2019.

[38] Z. He and C. Liu, "A compact high-efficiency broadband rectifier with a wide dynamic range of input power for energy harvesting," *IEEE Microw. Wireless Compon. Lett.*, vol. 30, no. 4, pp. 433–436, Apr. 2020.

[39] D.-A. Nguyen and C. Seo, "Design of high-efficiency broadband rectifier with harmonic control for wireless power transfer and energy harvesting," *IEEE Microw. Wireless Compon. Lett.*, vol. 32, no. 10, pp. 1231–1234, Oct. 2022.

[40] G. T. Bui, D.-A. Nguyen, and C. Seo, "A highly efficient design of broadband rectifier with harmonic suppression transferring for energy harvesting and wireless power transfer," *IEEE Microw. Wireless Technol. Lett.*, vol. 33, no. 7, pp. 1059–1062, Jul. 2023.

[41] D. Lee and J. Oh, "Broad dual-band rectifier with wide input power ranges for wireless power transfer and energy harvesting," *IEEE Microw. Wireless Compon. Lett.*, vol. 32, no. 6, pp. 599–602, Jun. 2022.

[42] S. Yu, F. Cheng, C. Gu, C. Wang, and K. Huang, "Compact and efficient broadband rectifier using T-type matching network," *IEEE Microw. Wireless Compon. Lett.*, vol. 32, no. 6, pp. 587–590, Jun. 2022.

[43] W. Liu, K. Huang, T. Wang, J. Hou, and Z. Zhang, "A compact high-efficiency RF rectifier with widen bandwidth," *IEEE Microw. Wireless Compon. Lett.*, vol. 32, no. 1, pp. 84–87, Jan. 2022.

[44] H. Lin, X. Chen, Z. He, Y. Xiao, W. Che, and C. Liu, "Wide input power range X-band rectifier with dynamic capacitive self-compensation," *IEEE Microw. Wireless Compon. Lett.*, vol. 31, no. 5, pp. 525–528, May 2021.

[45] S.-P. Gao and H. Zhang, "Topology comparison of single-diode rectifiers: Shunt diode vs. series diode," in *Proc. 12th Int. Workshop Electromagn. Compat. Integr. Circuits (EMC Compo)*, Oct. 2019, pp. 177–179.

[46] J. O. McSpadden, L. Fan, and K. Chang, "Design and experiments of a high-conversion-efficiency 5.8-GHz rectenna," *IEEE Trans. Microw. Theory Techn.*, vol. 46, no. 12, pp. 2053–2060, Dec. 1998.

[47] T.-W. Yoo and K. Chang, "Theoretical and experimental development of 10 and 35 GHz rectennas," *IEEE Trans. Microw. Theory Techn.*, vol. 40, no. 6, pp. 1259–1266, Jun. 1992.

[48] X. Liu, Y. Liu, S. Li, F. Wu, and Y. Wu, "A three-section dual-band transformer for frequency-dependent complex load impedance," *IEEE Microw. Wireless Compon. Lett.*, vol. 19, no. 10, pp. 611–613, Oct. 2009.

[49] Y. Cui, R. Li, and P. Wang, "A novel broadband planar antenna for 2G/3G/LTE base stations," *IEEE Trans. Antennas Propag.*, vol. 61, no. 5, pp. 2767–2774, May 2013.

GIA THANG BUI (Graduate Student Member, IEEE) received the B.Sc.(Eng.) degree from the School of Electronics and Telecommunication, Hanoi University of Science and Technology, Hanoi, Vietnam, in 2021, and the M.Sc.(Eng.) degree from the Department of Information and Telecommunications Engineering, Soongsil University, Seoul, South Korea, in 2023, where he is currently pursuing the Ph.D. degree.

His research interests include microwave wireless power transfer, microwave rectifiers, high input power rectifiers, microwave power amplifiers, and low noise amplifiers.

DANG-AN NGUYEN (Graduate Student Member, IEEE) was born in Thanh Hoa, Vietnam. He received the degree from the School of Electronics and Telecommunications, Hanoi University of Science and Technology (HUST), Vietnam, in 2016, and the Ph.D. degree from Soongsil University, South Korea, in 2023, where his major relates to microwave signal processing, radar systems, power amplifiers, rectifiers, and non-foster circuits.

He had three years of experience working as a Senior Member of the Signal Processing and Radio Communication Laboratory, HUST.

CHULHUN SEO (Senior Member, IEEE) received the B.S., M.S., and Ph.D. degrees from Seoul National University, Seoul, South Korea, in 1983, 1985, and 1993, respectively.

From 1993 to 1995, he was a Technical Staff Member with the Massachusetts Institute of Technology (MIT), Cambridge, MA, USA. From 1993 to 1997, he was an Assistant Professor with Soongsil University, Seoul. From 1999 to 2001, he was a Visiting Professor with MIT. From 1997 to 2004, he was an Assistant Professor with Soongsil University, where he has been a Professor of electronic engineering, since 2004. He is currently the Director of the Wireless Power Transfer Research Center, Seoul, supported by the Korean Ministry of Trade, Industry, and Energy, and the Director of the Metamaterials Research Center, Seoul, supported by Basic Research Laboratories through NRF Grant funded by MSIP. His research interests include wireless communication technologies, RF power amplifiers, and wireless power transfer using metamaterials. He served as the Chairperson for the IEEE MTT Korea Chapter, from 2011 to 2014.